CHEMISTRY OF MATERIALS

pubs.acs.org/cm

Article

Polymer-Ligated Uniform Lead Chalcogenide Nanoparticles with Tunable Size and Robust Stability Enabled by Judiciously Designed Surface Chemistry

Shuang Liang, Mingyue Zhang, Yanjie He, Zhitao Kang, Mengkun Tian, Meng Zhang, Han Miao, and Zhiqun Lin*

Cite This: *Chem. Mater.* 2021, 33, 6701−6712

Read Online

ACCESS | Metrics & More | Article Recommendations | Supporting Information

ABSTRACT: Despite recent progress in synthesis, self-assembly, and utility of low band gap lead chalcogenide nanoparticles (NPs) due to their intriguing optoelectronic characteristics, their compositional instability in ambient condition remains a great challenge for long-term practical applications. Herein, we report a unique strategy via capitalization on a set of starlike block copolymers as nanoreactors for in situ crafting of uniform lead chalcogenide NPs with readily tailored sizes, surface chemistry, near-infrared (NIR) optoelectronic properties, and more importantly, markedly enhanced stability against air exposure. The intimate and permanent tethering of the outer blocks of starlike block copolymers on the surface of lead chalcogenide NPs imparts their effective dispersion in both the solution and dry state. The diameter of the resulting NPs can be conveniently tuned by regulating the molecular weight (i.e., length) of the inner hydrophilic blocks of starlike block copolymers, manifesting the progressive red shift in the NIR absorption and emission as the diameter of the NPs increases. Most intriguingly, judiciously alternating the compositions and chain lengths of the outer blocks of the starlike block copolymers renders remarkably improved stability of lead chalcogenide NPs in ambient condition, representing no spectral change in both position and intensity for 30 days as compared to rapid and complete quenching of emission in 1 day in conventional small-molecular-ligand-capped counterparts. In principle, our starlike block copolymer nanoreactor strategy can be easily extended to synthesize functional NPs other than metal chalcogenides for investigation into their dimension-dependent physical properties and self-assembly as well as various applications.

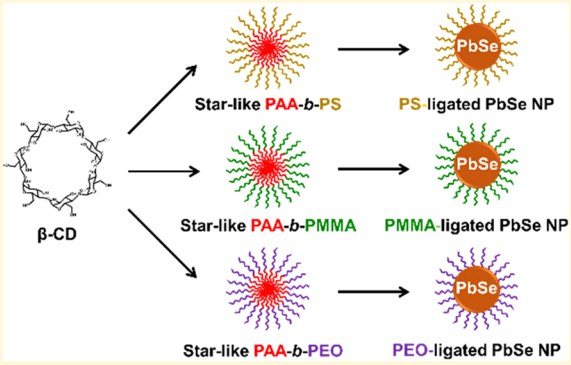

INTRODUCTION

The ability to precisely control the size, shape, and surface chemistry of colloidal nanoparticles (NPs) is the key to exploring their intriguing properties (e.g., optical, optoelectronic, catalytic, and magnetic properties) that depend heavily on these parameters[1−4] for a wide range of applications.[5,6] Recent advances in the colloidal synthesis of semiconducting metal chalcogenide NPs (e.g., CdSe, PbSe, and SnSe) enable their use in solar cells,[7] thermoelectric devices,[8,9] photodetectors,[10] etc. Among them, lead chalcogenide NPs have garnered much attention because of their broad size-tailorable optoelectronic properties in the visible to near-infrared (NIR) region,[3] large exciton Bohr radius,[11] and high carrier multiplication efficiency.[12] The latter renders the generation of multiple excitons via absorption of a single high-energy photon, thereby potentially increasing the photocurrent density that favors the optoelectronic applications.[7,10] Compared to the most widely studied PbS NPs, PbSe NPs possess a larger Bohr radius (i.e., 46 nm for PbSe vs 20 nm for PbS),[11] higher charge carrier mobility,[13] stronger quantum confinement effect,[14] broader tunable electronic band gap,[15] and greater carrier multiplication efficiency,[12] thus imparting enhanced performance of PbSe NPs-based optoelectronics.[16,17]

However, the long-term stability of PbSe NPs and durability of the materials and devices built upon them as building blocks are greatly plagued by the severe chemical instability of PbSe in ambient condition upon air exposure. Notably, PbSe NPs conventionally ligated with oleic acid (OA) are found to undergo rapid oxidation to yield oxides (i.e., PbO, $PbSeO_3$, and SeO_2) on the surface.[18] Consequently, the air-exposed PbSe NPs display the substantially altered band gap and quenching of the NIR photoluminescence (PL). In this context, several effective routes have been developed to alleviate such oxidation instability. The first approach involves

Received: March 31, 2021
Revised: May 29, 2021
Published: June 16, 2021

Downloaded via GEORGIA INST OF TECHNOLOGY on April 29, 2022 at 14:56:54 (UTC).
See https://pubs.acs.org/sharingguidelines for options on how to legitimately share published articles.

© 2021 American Chemical Society

https://doi.org/10.1021/acs.chemmater.1c01132
Chem. Mater. 2021, 33, 6701−6712

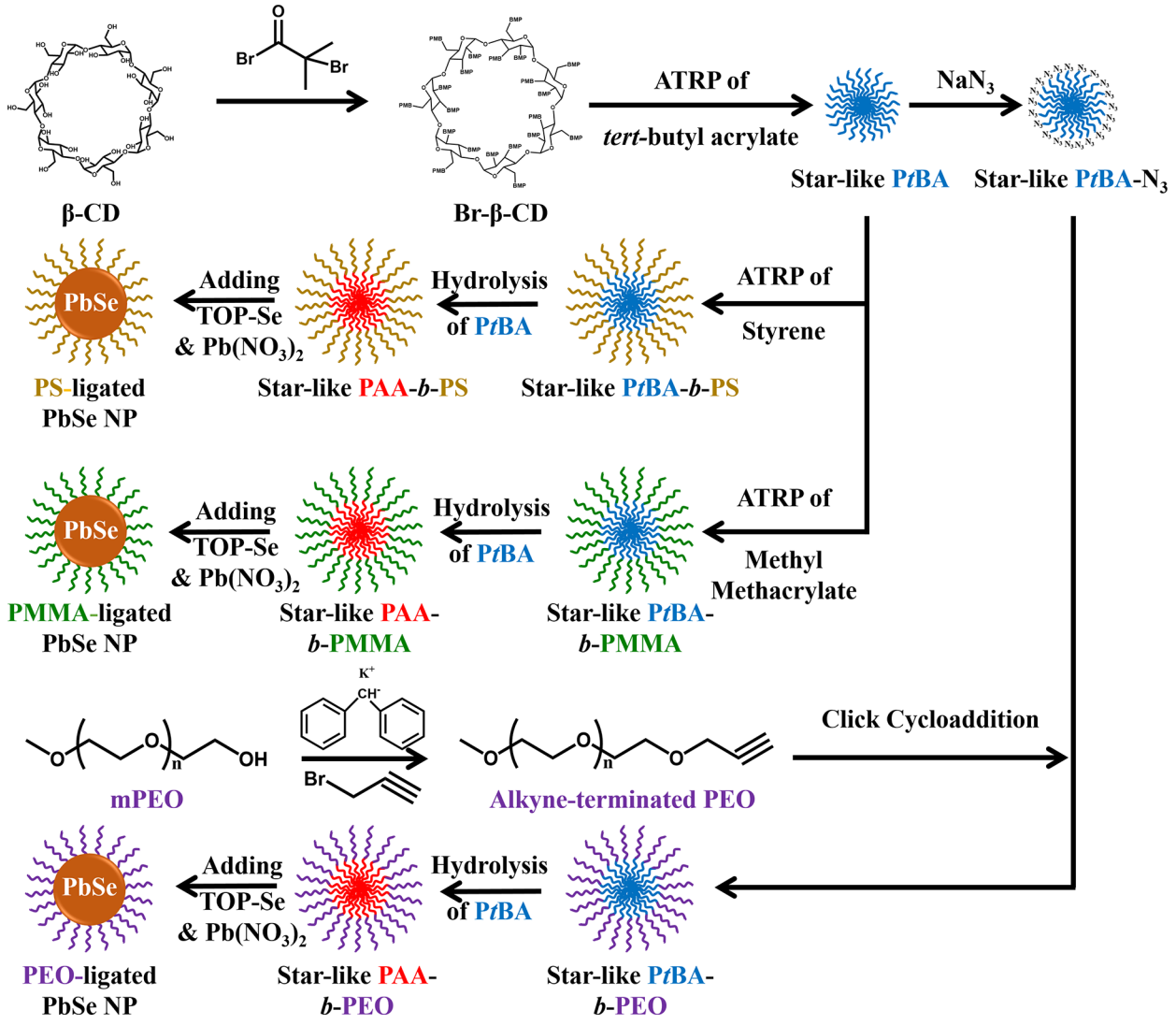

Figure 1. Stepwise representation of the synthesis of a PbSe nanoparticle with a tunable surface chemistry by capitalization on starlike PAA-*b*-PS (second row), PAA-*b*-PMMA (third row), and PAA-*b*-PEO (last row) block copolymers as nanoreactors. CD, cyclodextrin; BMP, 2-bromo-2-methylpropionate; TOP, trioctylphosphine.

the introduction of a higher band gap semiconductor shell over the PbSe surface to form a core/shell NP (e.g., PbSe/CdSe), leading to an enhanced stability of PbSe core against oxidation.[19] However, the larger band gap shell tends to hinder efficient charge transport. The second method invokes *in situ* and *ex situ* halide treatment of PbSe NPs to replace surface Se with halide atoms, thus forming a thin PbX_2 (X = Cl, Br, I) passivation layer that effectively prevents oxidation during the long course of air exposure and concurrently passivating surface trap states to increase the PL quantum yield.[14,20−22] Nevertheless, the PbX_2-passivated PbSe NPs exhibit different facets on the surface compared to pristine PbSe NPs, which may hinder the construction of superstructures based on these NPs.[22] The third way entails the use of phosphorus-containing ligands (e.g., tris(diethylamino)-phosphine,[23] diphenylphosphine,[14] and *n*-hexylphosphonic acid[23]) to introduce the P−O moieties from ligands onto the surfaces of PbSe NPs, facilitating efficient surface passivation and enhanced stability. Notably, it has been reported that introducing the P−O moieties may induce the lattice contraction and red shift of the excitonic transition energy of NPs.[24] It is important to note that as the surface-capping ligands (e.g., OA) coordinate with PbSe NPs, upon prolonged air exposure, surface-ligated ligands may dissociate from the NP surface, thereby resulting in incomplete surface coverage and unprotected surface atoms that potentially experience aggregation and oxidation and thus limited material stability and device durability. Clearly, it is highly desirable to develop a versatile strategy for producing PbSe NPs with controllable size, strongly bound yet tunable ligands, and superior air stability. This has yet to be largely explored.

Herein, we report a viable and robust route to *in situ* crafting of an array of PbSe NPs with precisely controlled diameters, permanently ligated polymer chains, tunable NIR optical properties, and greatly enhanced air stability via exploitation of a set of rationally designed starlike block copolymers as nanoreactors. First, starlike block copolymers with well-defined molecular weights of each block and narrow molecular distribution are synthesized by either sequential atom transfer radical polymerization (ATRP) or ATRP in conjunction with click reaction. They are poly(acrylic acid)-*block*-polystyrene (PAA-*b*-PS), poly(acrylic acid)-*block*-poly(methyl methacry-

https://doi.org/10.1021/acs.chemmater.1c01132
Chem. Mater. 2021, 33, 6701−6712

Table 1. Summary of the Molecular Weight and Polydispersity Index of Starlike Block Copolymers as Nanoreactors and the Corresponding Dimensions of the Polymer-Ligated PbSe NPs

samples	$M_{n,PAA}$[a] (g/mol)	$M_{n,PS}$[b] (g/mol)	$M_{n,PMMA}$[c] (g/mol)	$M_{n,PEO}$[d] (g/mol)	PDI[e]	diameter of PbSe NPs[f] (nm)
PAA-*b*-PS-1	3700	5100			1.10	4.1 ± 0.4
PAA-*b*-PS-2 (short PS)	4400	5100			1.12	5.2 ± 0.6
PAA-*b*-PS-3	7100	5100			1.16	8.3 ± 1.0
PAA-*b*-PMMA	4400		5300		1.13	5.1 ± 0.4
PAA-*b*-PEO	4400			5000	1.17	4.9 ± 0.5
PAA-*b*-PS-4 (intermediate PS)	4400	9200			1.15	5.1 ± 0.5
PAA-*b*-PS-5 (long PS)	4400	15400			1.16	5.2 ± 0.5

[a] $M_{n,PAA}$ is the MW of single-arm PAA calculated on the basis of ^{1}H NMR data from the MW difference between single-arm P*t*BA (before hydrolysis) and PAA (after hydrolysis) by following the equation below:

$$M_{n,PAA} = \frac{72.06}{128.17} \times M_{n,PtBA} = \frac{72.06}{128.17} \times \frac{A_b/9}{A_a/6} \times 128.17$$

where A_b and A_a are the integral area of the methyl protons in the *tert*-butyl group of the P*t*BA chain and the integral area of the methyl protons at the α-end of the P*t*BA chain in the ^{1}H NMR spectra, respectively. 128.17 and 72.06 are the MW of *t*BA monomer and AA repeat unit, respectively. [b] $M_{n,PS}$ is the MW of single-arm PS calculated on the basis of ^{1}H NMR data by following the equation below:

$$M_{n,PS} = \frac{A_c/5}{A_a/6} \times 104.15$$

where $M_{n,PS}$ is the MW of single-arm PS, A_c and A_a are the integral areas of phenyl protons on the PS block and methyl protons at the α-end of the single-chain block copolymer, respectively, and 104.15 is the molecular weight of the St monomer. [c] $M_{n,PMMA}$ is the MW of the single-arm PMMA calculated on the basis of ^{1}H NMR data by following the equation below:

$$M_{n,PMMA} = \frac{A_d/3}{A_a/6} \times 100.12$$

where $M_{n,PMMA}$ is the MW of single-arm PMMA, A_d and A_a are the integral areas of methoxy protons of the PMMA block and the methyl protons at the α-end of the single-chain block copolymer, respectively, and 100.12 is the molecular weight of the MMA monomer. [d] $M_{n,PEO}$ is the MW of the single-arm PEO obtained from DMF GPC prior to the "click" reaction. [e] PDI of the polymer was recorded by DMF GPC. [f] The dimensions of the resulting PbSe NPs were determined by performing image analysis on the TEM images.

late) (PAA-*b*-PMMA), and poly(acrylic acid)-*block*-poly(ethylene oxide) (PAA-*b*-PEO). Subsequently, because of the strong coordination interaction between the carboxylic groups of PAA blocks and metal precursors in conjunction with the selective partitioning of precursors in the compartment occupied by the inner hydrophilic PAA blocks, the implementation of these starlike block copolymers as nanoreactors *in situ* yields PbSe NPs perpetually ligated by hydrophobic PS and PMMA blocks and hydrophilic PEO blocks, respectively (i.e., polymer-ligated NPs with different surface chemistries). In addition, uniform PbSe NPs of different diameters, governed by the length of the inner PAA blocks, can be reliably accessed via controlling the ATRP reaction time. This in turn renders intriguing size-dependent optical properties of the resulting polymer-ligated PbSe NPs, displaying progressively red-shifted NIR absorption and emission with the increasing NP diameter. In stark contrast to conventional small-molecular-ligand-capped NPs, the outer polymer blocks (i.e., PS, PMMA, and PEO) intimately and permanently ligated on the surface of PbSe NPs as a result of original covalent binding to the inner PAA blocks, thereby ensuring outstanding colloidal stability by preventing possible ligand dissociation and thus NP aggregation over a long period of time. Most importantly, the outer polymer blocks also function as physical barriers to hinder oxygen diffusion, effectively alleviating surface oxidation of PbSe NPs upon air exposure. As such, strikingly improved air stability is achieved, representing considerably stable NIR absorption and emission (i.e., no spectral changes for 30 days) over the small-molecular-ligand-capped counterparts (complete quenching in 1 day only). The synthesis of metal chalcogenide NPs (i.e., CdSe and PbTe) other than PbSe are also demonstrated. Clearly, our starlike block copolymer nanoreactor strategy is effective and robust, enabling *in situ* creation of a variety of uniform metal chalcogenide NPs possessing controllable diameters, tunable NIR optical properties, tailorable surface chemistry, and significant air stability.

RESULTS AND DISCUSSION

As depicted in Figure 1, β-cyclodextrin (β-CD) with 21 hydroxyl groups was first esterificated by reacting with 2-bromo isobutyl bromide to yield brominated β-CD (denoted Br-β-CD). Nearly 100% conversion of the hydroxyl groups to ω-bromide terminals was confirmed by ^{1}H nuclear magnetic resonance (NMR) spectroscopy (see Figure S1 of the Supporting Information). Afterward, the brominated β-CD was used as a macroinitiator for the sequential ATRP of *tert*-butyl acrylate (*t*BA) and styrene (St) (i.e., yielding starlike poly(*tert*-butyl acrylate)-*block*-polystyrene (P*t*BA-*b*-PS)), followed by the hydrolysis of the inner poly(*tert*-butyl acrylate) (P*t*BA) blocks into PAA to form starlike PAA-*b*-PS (see Experimental Section).[25,26] Figures S2−S4 show the ^{1}H NMR spectra of as-prepared starlike P*t*BA, P*t*BA-*b*-PS, and PAA-*b*-PS. All of the as-prepared starlike block copolymers exhibit monomodal gel permeation chromatography (GPC) traces and narrow molecular weight (MW) distribution (i.e., polydispersity index, PDI < 1.2) without any linear polymer

https://doi.org/10.1021/acs.chemmater.1c01132
Chem. Mater. 2021, 33, 6701−6712

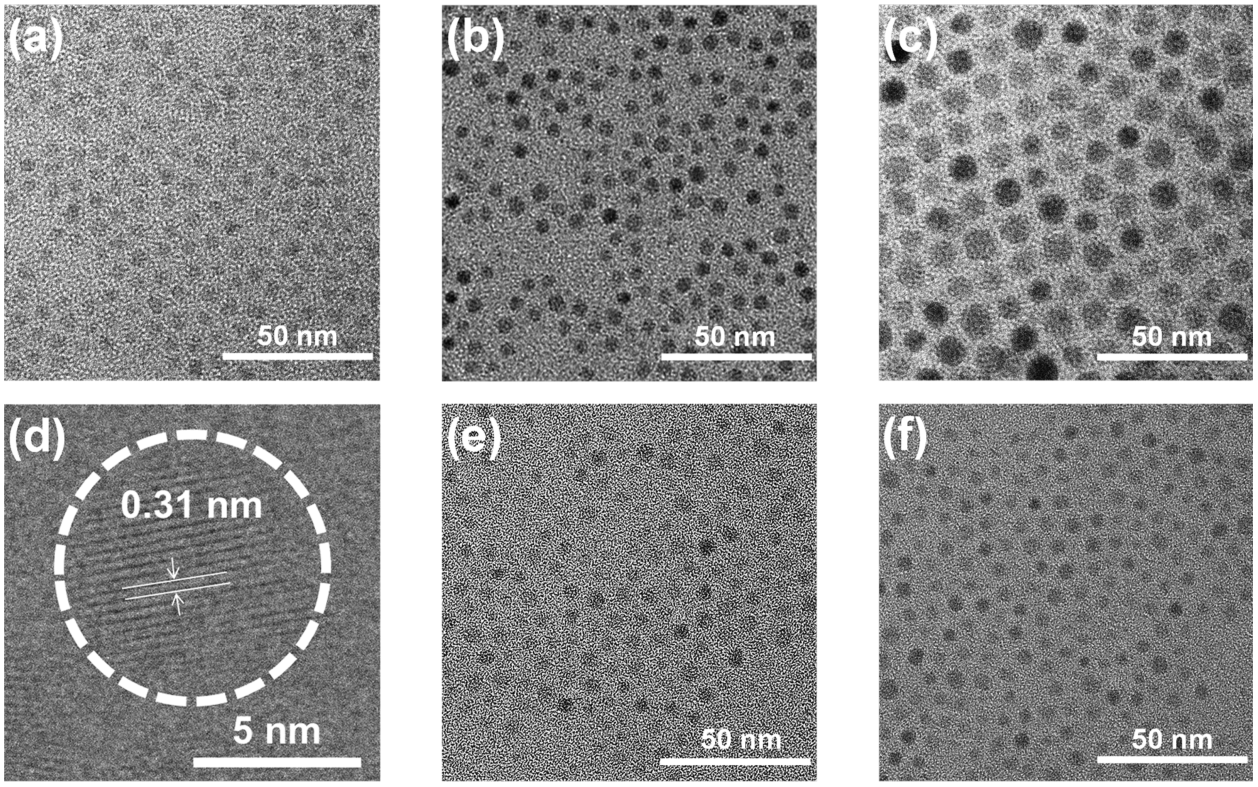

Figure 2. TEM images of PS-ligated PbSe NPs: (a) diameter, $D = 4.1 \pm 0.4$ nm, (b) $D = 5.2 \pm 0.6$ nm, and (c) $D = 8.3 \pm 1.0$ nm. They are crafted by using PAA-*b*-PS-1, PAA-*b*-PS-2, and PAA-*b*-PS-3 as nanoreactors, respectively (Table 1). (d) High-resolution TEM (HRTEM) image of PS-ligated PbSe NPs ($D = 8.3 \pm 1.0$ nm; the white circle is a guide to the eyes). TEM images of (e) PMMA-ligated PbSe NPs ($D = 5.1 \pm 0.4$ nm; templated by PAA-*b*-PMMA, Table 1) and (f) PEO-ligated PbSe NPs ($D = 4.9 \pm 0.5$ nm; templated by PAA-*b*-PEO, Table 1).

byproduct (Figure S5 and Table 1). It is also important to note that the symmetric peaks observed in the GPC traces suggest the absence of intermolecular coupling during the ATRP reactions.[27] Moreover, in sharp contrast to the conventional linear block copolymer, our starlike PAA-*b*-PS possesses 21 arms of PAA-*b*-PS block copolymer that covalently linked to the Br-*β*-CD core, forming a uniform unimolecular micelle in *N*,*N*-dimethylformamide (DMF) as confirmed by dynamic light scattering (DLS) measurement (Figure S6 and Table S1).

Subsequently, amphiphilic starlike PAA-*b*-PS block copolymers were utilized as nanoreactors to direct the synthesis of uniform PbSe NPs. Specifically, starlike PAA-*b*-PS block copolymers were first dissolved in DMF, which is a good solvent for both PAA and PS blocks to form a stable unimolecular micelle, followed by introduction of PbSe precursors (i.e., lead nitrate ($Pb(NO_3)_2$) and TOP-Se; second row in Figure 1). Upon the addition of benzyl alcohol (BA), which is a good solvent for inner PAA blocks but a poor solvent for the outer PS blocks, the uniform PAA-*b*-PS transitioned into the micelle with expanded inner PAA blocks and collapsed outer PS blocks.[28] As a result, the precursors are selectively loaded into the compartment occupied by the inner expanded PAA blocks owing to a strong coordination interaction between the carboxylic acid groups of PAA and metal moieties of the precursors, leading to the formation of PbSe NPs after refluxing at 160 °C. In addition, the outer PS blocks, originally covalently connected to the inner PAA blocks, are intimately and perpetually ligated on the surface of the resulting PbSe NP (i.e., forming PS-ligated PbSe NP; second row in Figure 1).

Figure 2a–c shows representative transmission electron microscopy (TEM) images of PS-ligated PbSe NPs with average diameters of 4.1 ± 0.4, 5.2 ± 0.6, and 8.3 ± 1.0 nm, respectively, templated by starlike PAA-*b*-PS nanoreactors (PAA-*b*-PS-1, PAA-*b*-PS-2, and PAA-*b*-PS-3, respectively, in Table 1). Owing to the controlled "living" characteristic of ATRP, the MW of the inner PAA blocks and thus the diameter of the PbSe NPs can be readily tailored by varying the ATRP time of the P*t*BA blocks that are hydrolyzed into PAA later. As shown in Table 1, it is important to note that PAA-*b*-PS-1, PAA-*b*-PS-2, and PAA-*b*-PS-3 all possess the same MW of PS blocks as the outer blocks, suggesting the diameter of PbSe NPs is dictated by the length of the inner hydrophilic PAA blocks via the coordination interaction noted above, and the outer PS blocks function only as the capping ligands that are tethered on the surface of the PbSe NP. High-resolution TEM (HRTEM) shows a lattice spacing of 0.31 nm, corresponding to the (220) interplanar distance of face-centered cubic-phased PbSe (Figure 2d). In addition, the energy-dispersive X-ray analysis further confirmed the 1:1 atomic ratio between Pb and Se (Figures S7 and S8 and Table S2). In addition to PbSe, other metal chalcogenide NPs (i.e., CdSe and PbTe) were also synthesized using PAA-*b*-PS-3 as a nanoreactor (Table 1), clearly demonstrating the effectiveness and versatility of our starlike block copolymer nanoreactor strategy in crafting a variety of NPs of interest (Figure S9).

Furthermore, the growth kinetics of the PbSe NPs template by starlike block copolymer nanoreactors (i.e., PAA-*b*-PS-3 in Table 1) was monitored by TEM (Figure S10). Specifically, after heating at 160 °C for 60 min, small nuclei (~3 nm) of PbSe formed. While the reaction temperature was maintained

https://doi.org/10.1021/acs.chemmater.1c01132
Chem. Mater. 2021, 33, 6701−6712

at 160 °C, the diameter of the PbSe NPs increased to 5−6 nm at 120 min and 7−8 nm at 180 min. However, further prolongation of the reaction time to 240 min did not yield PbSe NPs with a diameter over 9 nm, which may be due to the inability of the outer PS blocks of the nanoreactors to coordinate with PbSe precursors. Thus, differing from those of the conventional approach,[22] the results shown in Figure S10 suggest the size of the PbSe NPs crafted by utilizing the starlike block copolymers as nanoreactors is determined by the size of the inner PAA blocks of the nanoreactors.

For substantiation of the formation of PbSe NPs that was indeed directed by starlike block copolymer nanoreactors, two control experiments for PbSe NPs were conducted with identical reaction parameters and conditions, except one without the use of starlike block copolymer nanoreactors and the other with linear PAA-*b*-PS block copolymers as nanoreactors. It is not surprising that, in the absence of any block copolymer nanoreactors, the nucleation and growth of PbSe NPs had no spatial confinement, thus leading to an irregular morphology and large-sized particles (Figure S11a). On the other hand, with linear PAA-*b*-PS block copolymers as nanoreactors, the micelles originating from the self-assembly of linear block copolymers were not thermodynamically stable and likely dissociated at a high temperature in our study (i.e., 160 °C), thereby forming aggregates instead of NPs (Figure S11b).

In addition, the ligating of PS blocks on the surface of a PbSe NP can be confirmed by preferentially staining the PS chains with RuO_4 vapor. Specifically, the 5 nm short PS-ligated PbSe NPs (synthesized using PAA-*b*-PS-2 in Table 1) toluene solution was dropped onto a TEM grid, followed by the exposure to RuO_4 vapor. The representative TEM image of PS-ligated PbSe NP after staining is shown in Figure S12. Intriguingly, one can see that a layer of PS intimately covered the surface of the 5 nm PbSe NP. Moreover, the comparable molecular weights of PAA and PS blocks (PAA-*b*-PS-2 in Table 1) yield a similar thickness of PS shell to that of the PbSe core radius. On the other hand, it is notable that the diameter of the PbSe/PS core/shell NPs in Figure S12 is 10.4 nm, which is also comparable to the hydrodynamic size of the PAA-*b*-PS-2 micelle (i.e., 10.8 nm) measured by DLS (Figure S6 and Table S1), providing direct evidence for the ligating of PS blocks on the surface of the PbSe NP. Thus, the formation of PbSe NPs was directed by the starlike block copolymer nanoreactors.

As discussed above, tailoring the surface chemistry of PbSe NPs after synthesis can improve their stability upon air exposure, as demonstrated in previous studies (i.e., forming core/shell NPs, passivation with PbX_2, and capping with phosphorus-containing ligands). In contrast, our starlike PAA-*b*-PS nanoreactors rendered *in situ* crafting of PS-ligated PbSe NPs possessing hydrophobic protective PS chains on the surface to prevent PbSe NPs from air exposure and oxidation, dispensing with the need for postsynthetic treatments as noted above. In this context, we also synthesized starlike PAA-*b*-PS with varied PS lengths (PAA-*b*-PS-4 and PAA-*b*-PS-5, Table 1), PAA-*b*-PMMA (PAA-*b*-PMMA, Table 1) and PAA-*b*-PEO (PAA-*b*-PEO, Table 1) block copolymers, as nanoreactors to scrutinize the effect of these outer polymer hairs of different lengths (for PS) and compositions (for PMMA and PEO) on the air stability of the resulting polymer-ligated NPs, as discussed later. Nonetheless, the synthesis of starlike PAA-*b*-PMMA (third row, Figure 1; see Experimental Section) was similar to that of PAA-*b*-PS. The successful synthesis of starlike P*t*BA-*b*-PMMA and PAA-*b*-PMMA was confirmed by ^{1}H NMR (Figures S13 and S14). On the other hand, the *ω*-bromide terminals of starlike P*t*BA can be converted into azide groups by an S_N2 reaction using NaN_3, as confirmed by the appearance of a band centered at 2100 cm^{-1} in the Fourier-transform infrared (FT-IR) spectrum (Figure S15), which is characteristic of the stretching of the $-N_3$ group. Afterward, alkyne-terminated PEO synthesized by nucleophilic substitution of the PEO methyl ether (mPEO) were clicked onto azide-terminated starlike P*t*BA through copper(I)-catalyzed alkyne−azide click cycloaddition reaction, as verified by ^{1}H NMR (Figure S16), followed by hydrolysis of the inner PtBA blocks to yield starlike PAA-*b*-PEO (last row, Figure 1; see Experimental Section), as substantiated by ^{1}H NMR (Figure S17).

Subsequently, PAA-*b*-PMMA and PAA-*b*-PEO were utilized as nanoreactors for the synthesis of PbSe NPs using DMF as a good solvent, and BA as a poor solvent for PMMA and diphenyl ether (DPE) as a poor solvent for PEO, respectively (see Experimental Section). It is noteworthy that both starlike PAA-*b*-PMMA and PAA-*b*-PEO possess the same MW of the inner PAA blocks as that of starlike PAA-*b*-PS (PAA-*b*-PS-2; Table 1). Thus, the resulting PMMA-ligated and PEO-ligated PbSe NPs displayed similar diameters, that is, D = 5.1 ± 0.4 nm for PMMA-ligated NPs (Figure 2e) and D = 4.9 ± 0.5 nm for PEO-ligated NPs (Figure 2f), as that of PS-ligated NPs (D = 5.2 ± 0.6 nm). The X-ray diffraction (XRD) patterns of PS-ligated, PEO-ligated, and PMMA-ligated PbSe NPs can be indexed to the face-centered cubic phase of PbSe (Figure 3a), which is consistent with the standard XRD profile of PbSe and

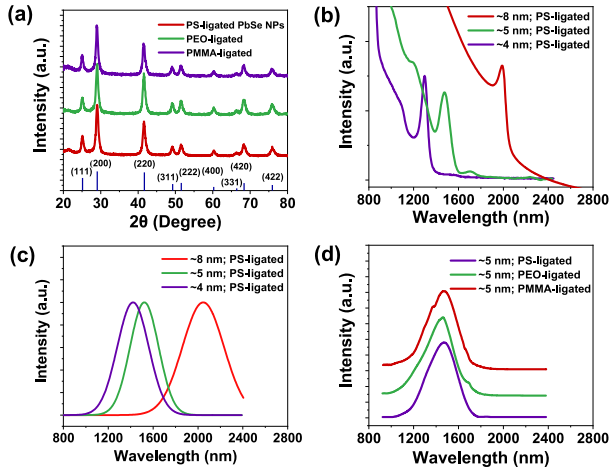

Figure 3. (a) X-ray diffraction (XRD) profile of PbSe NPs ligated with PS, PEO, and PMMA. The dark blue lines represent the standard XRD profile of PbSe (JCPDS No. 06-0354). (b) Near-infrared (NIR) absorption spectra of PbSe NPs with diameters of 4.1 ± 0.4, 5.2 ± 0.6, and 8.3 ± 1.0 nm (templated by PAA-*b*-PS-1, PAA-*b*-PS-2, and PAA-*b*-PS-3, respectively; Table 1). (c) NIR PL spectra of the three PbSe NPs in (b). (d) NIR PL spectra of PbSe NPs with nearly identical diameters yet different surface-ligated polymers (i.e., PS, PEO ,and PMMA, templated by PAA-*b*-PS-2, PAA-*b*-PMMA, and PAA-*b*-PEO; Table 1). The shoulder peaks located around 1700 nm for PEO-ligated and PMMA-ligated PbSe NPs were due to the residual hexane (poor solvent) used for purification (see Experimental Section). The shoulder peak around 1400 nm for PMMA-ligated PbSe NPs was due to the residual toluene (good solvent) used for purification (see Experimental Section).

https://doi.org/10.1021/acs.chemmater.1c01132
Chem. Mater. 2021, 33, 6701−6712

the HRTEM result (Figure 2d). Moreover, the capping of PbSe NPs with hydrophilic PEO rendered their water solubility (Figure S18).

Interestingly, the polymer-ligated uniform PbSe NPs of different diameters were found to exhibit size-dependent NIR optical properties (Figure 3b−d) as a result of their intrinsic small band gap and quantum confinement effect.[15] Because of the large Bohr radius of PbSe (46 nm),[11] downsizing the PbSe NPs from 8.3 ± 1.0, to 5.2 ± 0.6, to 4.1 ± 0.4 nm (Figure 2a−c) led to an increased quantum confinement effect, imparting a blue shift of the first exciton peak position of absorption spectra (i.e., from 1985 nm of 8.3 nm NPs, to 1472 nm of 5.2 nm NPs, to 1297 nm of 4.1 nm NPs; Figure 3b) and PL peak position (i.e., from 2040 nm of 8.3 nm NPs, to 1522 nm of 5.2 nm NPs, to 1421 nm of 4.1 nm NPs; Figure 3c), which is comparable to the results found in the literature.[29−31] The nonzero background in the long-wavelength region (i.e., over 2100 nm) of the NIR absorption in Figure 3b of 8 nm PS-ligated PbSe NPs may originate from the presence of weak Rayleigh scattering in low-concentration PbSe solutions.[32] In addition to the TEM images shown in Figure 2, the uniformity of NPs was further demonstrated by the sharp first exciton peak in the absorption spectra for all three PS-ligated PbSe NPs (Figure 3b),[14] which would otherwise yield a broad absorption peak. It is also notable that altering the surface capping ligands of PbSe NPs from PS to PEO and PMMA (Figure 3d) or increasing the MW of the outer PS blocks (Figure S19) invoked no discernible change in their PL spectra, further corroborating the sizes of as-crafted PbSe NPs are identical and determined only by the MW of the inner PAA blocks.

Intrigued by the size-dependent NIR optical properties of polymer-capped PbSe NPs discussed above and with the goal of achieving long-stability PbSe NPs for optoelectronics, we set out to scrutinize the stability of as-crafted polymer-capped PbSe NPs under ambient condition by tracking their NIR absorption and PL spectra in trichloroethylene (TCE) over time (Figure 4a,b). For comparison, we also synthesized conventional OA-ligated PbSe NPs with an average diameter of ∼5 nm (Figure S20a).[22] After they were stored in ambient condition for up to 30 days, no obvious change in peak shape and position coud be seen in both NIR absorption spectra and PL spectra. This contrasts sharply with the apparent blue shift in the NIR absorption spectrum of OA-ligated PbSe NPs after only 1 day of ambient storage (Figure S20b), which can be attributed to surface oxidation and thus the decreased size of PbSe NPs.[18,33]

The appearance of sharp peaks in the XRD profiles (Figure S21a) of both PS-ligated and OA-ligated PbSe NPs suggest good crystallinity of both PbSe NPs synthesized from different approaches. Moreover, as shown in Figure S21b, the peaks centered at 41.7° (i.e., the (220) facet) for PbSe NPs with different surface chemistries possess similar full-width at half-maximum (fwhm), suggesting the OA-ligated PbSe NPs manifest similar crystallinity to the PS-ligated PbSe NPs. On the other hand, the decreased grafting density of a surface ligand has been found to trigger the instability of the morphology and optical properties of PbSe NPs.[34] Notably, the calculated PS grafting density on the surface of the 5 nm PbSe NP is only 0.267 PS chain per nm^2 ((PS grafting density = $21/(\pi*D^2) = 21/(\pi*5^2) \approx 0.267$ PS chains per nm^2, where D is the diameter of the PbSe NP), which is significantly lower than the grafting density of OA in OA-ligated PbSe NPs (i.e., 2−3 oleate ligand per nm^2).[22,35] Therefore, on the basis of the comparison of the crystallinity and surface ligand grafting density, we conclude that the robust stability of polymer-ligated PbSe NPs is not due to the difference in crystallinity and surface ligand grafting density from the OA-ligated PbSe NPs.

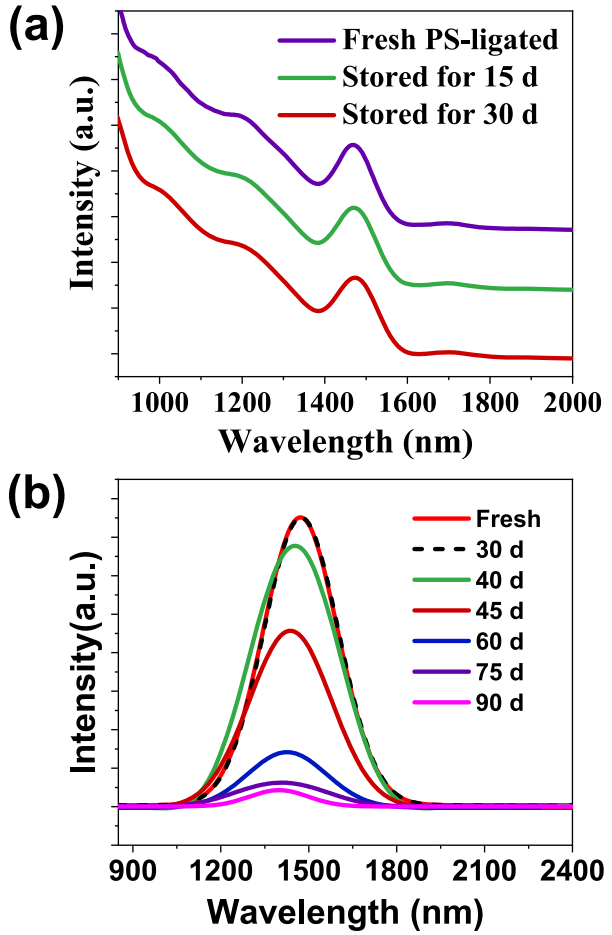

Figure 4. (a) NIR absorption spectra of PS-ligated PbSe NPs (D = 5.2 ± 0.6 nm; crafted using PAA-*b*-PS-2, Table 1) as a function of time after being stored in ambient condition for 30 days. (b) NIR PL spectra of PS-ligated PbSe NPs (D = 5.2 ± 0.6 nm; crafted using PAA-*b*-PS-2, Table 1) as a function of time during a course of 90-day storage in ambient condition.

Figure 5 compares the X-ray photoelectron spectroscopy (XPS) of pristine PbSe NPs and air-exposed PbSe NPs, revealing the salient difference between PS-ligated PbSe NPs and conventional OA-ligated PbSe NPs after exposure to air. The XPS spectra in Figure 5 have been calibrated with the binding energy of the peak in the C 1s level assigned to 284.5 eV, which can be seen in Figure S22. Prior to air exposure, the freshly prepared OA-ligated and PS-ligated PbSe NPs displayed similar peaks in all Pb 4f, Se 3d, and O 1a levels. Specifically, in the Pb 4f level, the two peaks at ∼137 and ∼142 eV are from the $4f_{5/2}$ and $4f_{7/2}$ spin−orbit coupled doublet of Pb, indicating Pb^{2+} ions in PbSe NPs.[18] However, after air exposure, two additional peaks at 139 and 144 eV appeared in OA-ligated PbSe NPs, but were not found in PS-ligated PbSe NPs, suggesting the formation of the Pb−O bond that has higher energy than that of the Pb−Se bond in OA-ligated PbSe NPs,[18] but not in PS-ligated PbSe NPs. On the other hand, in the Se 3d level, pristine PbSe NPs manifested only two peaks

https://doi.org/10.1021/acs.chemmater.1c01132
Chem. Mater. 2021, 33, 6701−6712

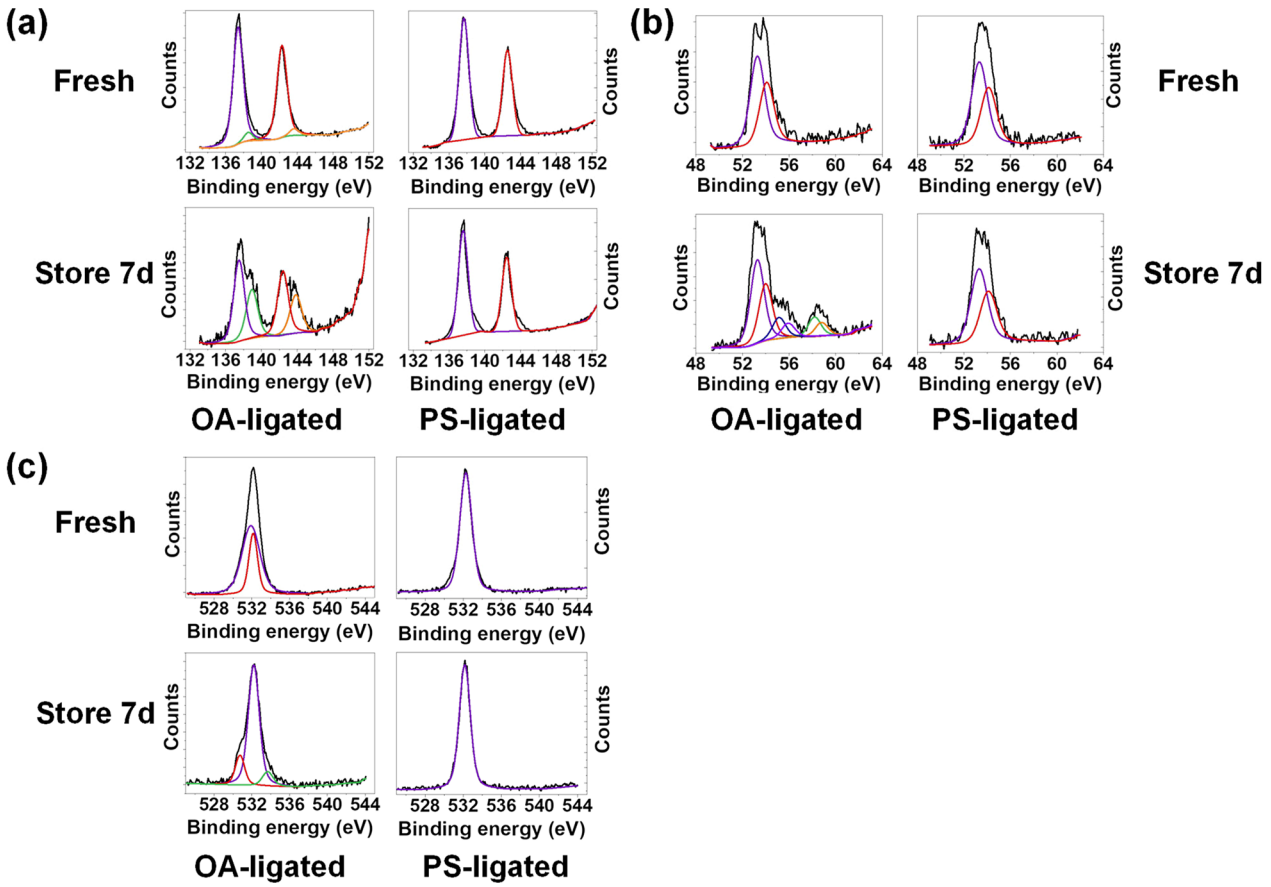

Figure 5. X-ray photoelectron spectroscopy (XPS) profiles of (a) Pb 4f, (b) Se 3d, and (c) O 1s levels of OA-ligated and PS-ligated PbSe NPs before and after being stored in ambient conditions for 7 days.

at ∼53 and ∼54 eV because of the spin−orbit splitting of the Se^{2-} 3d core level into $3d_{5/2}$ and $3d_{3/2}$ levels.[22,36] The air exposure resulted in the generation of additional peaks from ∼55 to ∼60 eV in OA-ligated PbSe NPs, signifying the formation of SeO_2 and SeO_3^{2-} moieties due to the oxidation of Se^{2-} on the surface of PbSe NPs;[18,22] however, no new peak emerged at the Se 3d level of air-exposed PS-ligated PbSe NPs. The formation of two extra peaks at ∼530 and ∼534 eV at the O 1s level of air-exposed OA-ligated PbSe NPs further substantiated the formation of lead oxides on the surface of PbSe NPs.[22,37]

This result demonstrated that the surface-ligated polymers account for the enhanced stability due to the greatly retarded surface oxidation of PbSe NPs. However, further prolonged ambient storage from 30 to 90 days witnessed a continuous drop in the NIR PL peak intensity associated with a blue shift (i.e., from 1472 nm in a freshly prepared sample to 1413 nm at 90 days; approximately 35 meV) of the PL peak position (Figure 4b).

Figure 6a presents the impact of the surface chemistry on the air stability of PbSe NPs by monitoring the relative PL intensity during ambient storage. The MWs of the outer blocks (PS, PMMA, and PEO; Table 1) were kept nearly identical to exclude the influence of the polymer chain length on the air stability of polymer-ligated PbSe NPs. For conventional OA-ligated PbSe NPs, the intensity of the PL peak rapidly dropped to only 0.3% of the original value after storage in ambient condition for 1 day, and completely quenched in 3 days. However, in stark contrast, the relative PL peak intensity for all polymer-ligated PbSe NPs remained above 90% after 1 day of storage under the same conditions. Particularly, the emission of PS-ligated PbSe NPs remained nearly unchanged for 30 days, gradually decreased afterward, and were still emissive after 90 days (∼10% of original intensity), outperforming PMMA-ligated and PEO-ligated PbSe NPs (Figure 3c). The latter two NPs were able to stay emissive for approximately 75 and 60 days, respectively. Taken together, the ligated polymers certainly promoted the stability of PbSe NPs against air exposure. Among them, PS manifested the most effectiveness in retarding the air oxidation of NPs over PMMA and PEO, which can be rationalized on the basis of Hansen solubility parameters of these polymers and the solvent used (i.e., TCE) (Table S3).

Hansen solubility parameters render the prediction of the solubility of one compound in another.[38] The Hansen parameter of each molecule has three different components, namely, dispersion force (σ_d), dipole−dipole (polar) interaction (σ_p), and hydrogen bonding (σ_h). These three components serve as the coordinates of a point in the so-called Hansen space. Moreover, in addition to the three coordinates that determine the position of a compound in Hansen space, the compound also possesses an intrinsic interaction radius (R_0) in the Hansen space that decides the radius of the solubility sphere of the compound. If the distance between the solvent and solute in Hansen space is smaller than the R_0 of the solute (i.e., the coordinates of the solvent locate within the solubility sphere of the solute), the solute is likely to be dissolved into the solvent. In this context, the distance (R_a)

https://doi.org/10.1021/acs.chemmater.1c01132
Chem. Mater. 2021, 33, 6701−6712

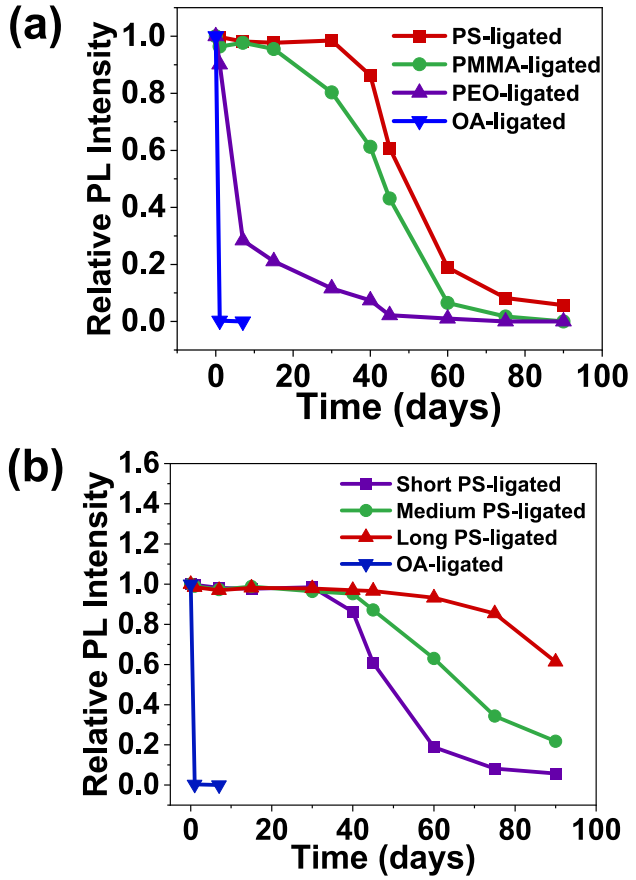

Figure 6. (a) Time-dependent evolution of relative NIR PL intensity for ∼5 nm PbSe NPs stored in ambient condition. They are ligated with conventional oleic acid (OA), PS (template by PAA-*b*-PS-2; Table 1), PMMA (templated by PAA-*b*-PMMA; Table 1), and PEO (template by PAA-*b*-PEO; Table 1), respectively. (b) Time-dependent evolution of relative NIR PL intensity for ∼5 nm PbSe NPs stored in ambient condition. They are ligated with PS of different chain lengths (short PS, PAA-*b*-PS-2; intermediate PS, PAA-*b*-PS-4; and long PS, PAA-*b*-PS-5, respectively, in Table 1).

of the solvent coordinates (σ_{d2}, σ_{p2}, σ_{h2}) to the solute coordinates (σ_{d1}, σ_{p1}, σ_{h1}) can be calculated according to the following equation:[38]

$$R_a^2 = 4(\delta_{d2} - \delta_{d1})^2 + (\delta_{p2} - \delta_{p1})^2 + (\delta_{h2} - \delta_{h1})^2 \quad (1)$$

The ratio of R_a/R_0 is known as the relative energy difference of the solvent−solute system. For $R_a/R_0 < 1$, the solute is highly likely to be dissolved in the specific solvent. In this context, the R_a/R_0 of three polymers (PMMA, PEO, and PS) with TCE were calculated, yielding 0.569 for PMMA with TCE, 0.2534 for PEO with TCE, and 0.8734 for PS with TCE (Table S3). This signifies that TCE is a good solvent for PMMA, PEO, and PS. As a result, all polymer-ligated PbSe NPs showed excellent colloidal stability in TCE (Figure S23).

Notably, the smaller R_a/R_0 (suggesting the more similar chemical structure of polymer to TCE) correlates to the higher solubility[35] of the polymer in TCE and in turn the expanded polymer chain conformation. As PEO has the smallest R_a/R_0 of 0.2534, the ligated PEO chains on the surface of a NP are fully expanded in TCE, resulting in a layer of loosely packed PEO chains on the surface of PbSe NP. This in turn provides a relatively fast pathway for the diffusion of dissolved oxygen molecules to reach the surface of PbSe NP, leading to surface oxidation and quenching of NIR PL of PbSe NPs. Compared to PEO, PMMA possesses a moderate R_a/R_0 of 0.569. As a result, the extent of PMMA chain expansion in TCE is less than PEO, imparting a denser packing of PMMA chains on the surface of a NP. This retards the diffusion of oxygen in TCE to NP and thus the reduced degree of surface oxidation over that of PEO-ligated NPs (Figure 6a). It is not surprising that an even denser packing of polymer chains outside the NP could further boost the air stability, as exemplified in the case of PS-ligated NPs due to the highest R_a/R_0 of 0.8734 among the three polymers ligated. For example, after a 75-day storage in ambient condition, PS-ligated PbSe NPs still manifested a 4.8-time PL intensity over that of PMMA-ligated PbSe NPs, whereas PEO-ligated PbSe NPs were fully quenched (Figure 6a).

Inspired by the high stability of PS-ligated PbSe NPs against air exposure over PEO- and PMMA-ligated ones, we further examined the effect of the PS chain length on the stability of PbSe NPs, as shown in Figure 6b. The MWs of single short, intermediate, and long PS chains are 5000 g/mol, 10000 g/mol, 15000 g/mol, respectively (Table 1). As the PS chain length increased, the relative PL intensity progressively enhanced, suggesting that the longer PS chains can essentially hinder the oxygen diffusion in TCE to the surface of the PbSe NP. For instance, after being stored in ambient condition for 90 days, the long and intermediate PS-ligated PbSe NPs exhibited approximately 10.8-fold and 3.8-fold NIR PL intensity over the short PS-ligated counterpart. However, it is also notable that long polymer-ligated PbSe NPs may carry limited electrical conductivity and thus not be suitable for some optoelectronic devices because of the insulating characteristic of polymers and inadequate electron tunneling. Nonetheless, this merits further study and will be pursued. Alternatively, introducing conjugated polymers as the outer blocks to craft conjugated polymer-ligated PbSe NPs may concurrently render improved conductivity and enhanced stability, which may also be our future research effort.[39−42]

CONCLUSIONS

In summary, we demonstrated the crafting of a family of polymer-ligated uniform metal chalcogenide NPs with readily tailored sizes, compositions, and surface chemistry via employing judiciously designed starlike block copolymers as nanoreactors. When the chain length of the inner PAA blocks were simply tuned during ATRP, the diameter of the NPs can be conveniently controlled, exhibiting size-dependent NIR optical properties because of quantum confinement effect. Notably, the outer polymer blocks of different types (i.e., PS, PMMA, and PEO) are permanently tethered on the surface of NPs, rendering tunable surface chemistry, excellent colloidal stability, and markedly enhanced air stability without the need for postsynthesis treatment. When the composition (and thus possessing varied solubility parameters) and chain length of the outer blocks were systematically engineered, PS-ligated PbSe NPs with long PS chain length manifest the highest air stability and the most stable NIR emission, even after being stored in ambient condition over 90 days. This contrasts sharply to the quenching of emission in conventional OA-ligated PbSe NPs in 1 day under the same condition. Compared to PEO- and PMMA-ligated ones, the outstanding stability of PS-ligated PbSe NPs is a direct consequence of the presence of protective PS chains with relatively denser packing, which are capable of functioning as more effective physical barriers to retard the

https://doi.org/10.1021/acs.chemmater.1c01132
Chem. Mater. 2021, 33, 6701−6712

diffusion of dissolved oxygen molecules to reach the surface of NP for oxidation. As such, our starlike block copolymer nanoreactor strategy affords a general and robust platform for creating functional NPs of interest to explore the size-dependent and surface-chemistry-enabled physical properties and stability for a diversity of applications in optics, electronics, optoelectronics, thermoelectrics, and catalysis, among other areas.

EXPERIMENTAL SECTION

Materials. Toluene (99.5%), dichloromethane (>99.5%), α-bromoisobutyryl bromide (BiBB, 98%), anisole (99%), 2-butanone (99.0%), anhydrous dimethylformamide (>99.8%), anhydrous 1-methyl-2-pyrrolidinone (NMP, 99.5%), *N*,*N*,*N*′,*N*′,*N*″-pentamethyldiethylene triamine (PMDETA, 99%), sodium azide (>99.5%), trifluoroacetic acid (TFA, 99.9%), lead(II) nitrate ($Pb(NO_3)_2$, 99.999%), selenium powder (∼100 mesh, 99.99%), OA (technical grade, 90%), TOP (97%), diethyl ether (anhydrous, 99.0%), ethanol (anhydrous, 99.5%), calcium hydride (CaH_2, for synthesis), sodium bicarbonate ($NaHCO_3$, 99.7%), aluminum oxide powder (activated, neutral, ∼325 mesh), tetrahydrofuran (THF, 99.0%), acetone (99.5%), magnesium sulfate ($MgSO_4$, anhydrous, 99.5%), potassium (chunks in mineral oil, 98%), naphthalene (99%), diphenylmethane (99%), hydrochloride acid (HCl, ACS reagent, 37%), propargyl bromide (80 wt % in toluene), ethyl α-bromoisobutyrate (EBiB, 98%), mPEO (Mn ∼ 5000 g/mol), TCE (ACS reagent, 99.5%), BA (anhydrous, 99.8%), DPE (99%), octadecene (ODE, technical grade, 90%), cadmium nitrate ($Cd(NO_3)_2$, 99.997%), tellurium powder (∼200 mesh, 99.8%), deuterated chloroform ($CDCl_3$, 99.96%), DMF-d_7 (99.5%), lithium bromide (LiBr, 99%), and acetic acid (99.7%) were purchased from Sigma-Aldrich and used as received.

β-CD (>97.0%, Sigma-Aldrich) was dried under vacuum for 48 h at 60 °C and azeotropic-distillated in toluene for 2 h at 120 °C prior to the esterification reaction. Copper(I) bromide (CuBr, 98%, Sigma-Aldrich) was stirred for 2 h in acetic acid, filtered, washed with ethanol and diethyl ether, and dried in vacuum at room temperature overnight. Styrene (99.9%, Sigma-Aldrich) and *t*BA (98%, Sigma-Aldrich) were distilled over CaH_2 under reduced pressure prior to use. MMA (99%, Sigma-Aldrich) was passed through a neutral, activated aluminum oxide powder column prior to use.

Synthesis of Heptakis[2,4,6-tri-O-(2-bromo-2-methylpropionyl]-β-cyclodextrin) (Br-β-CD Macroinitiator). Azeotropically distilled β-CD (2.5 mmol) was dissolved in 40 mL of anhydrous NMP at 0 °C. Subsequently, BiBB (105 mmol) was dropwise added to the β-CD solution under stirring in an hour. Afterward, the reaction solution was maintained at room temperature under stirring for 24 h. The solution was then diluted with 100 mL of dichloromethane and washed with saturated $NaHCO_3$ aqueous solution and deionized water three times. The product was retrieved from the solution by rotary evaporation. After it was redissolved in acetone, the Br-β-CD acetone solution was added to water for crystallization to remove impurities. The precipitant was then dissolved in dichloromethane, dried with anhydrous $MgSO_4$, and filtered. The final solid product was obtained by rotary evaporation to remove all of the solvent.

Synthesis of Hydrophobic Starlike Poly(tert-butyl acrylate) (Starlike PtBA). Br-β-CD was used as a macroinitiator for atom transfer radical polymerization (ATRP) of *t*BA. Specifically, Br-β-CD, CuBr, PMDETA, 2-butanone, and purified *t*BA (molar ratio = 1:1:2:1000:1000) were mixed in an ampule, degassed by three freeze−pump−thaw cycles in liquid nitrogen, and placed in an oil bath preheated at 60 °C for a desired time. Afterward, the polymerization was stopped by quenching in liquid nitrogen and exposure to air. The reaction solution was then diluted with acetone, passed through a neutral, activated aluminum oxide column to remove copper catalyst, and precipitated with a methanol/water (volume ratio = 1:1) mixture to obtain the final product. Finally, starlike P*t*BA was dried in vacuum at room temperature for 48 h.

Synthesis of Hydrophobic Starlike Poly(tert-butyl acrylate)-block-polystyrene (Starlike PtBA-b-PS). Starlike P*t*BA was used as the macroinitiator for ATRP of purified St monomer. Briefly, starlike P*t*BA, CuBr, PMDETA, St, and anisole (molar ratio = 1:1:2:1000:1000) were mixed in an ampule, degassed by three freeze−pump−thaw cycles in liquid nitrogen, and polymerized at 90 °C for a specific period of time. Afterward, the reaction was stopped by immersion in liquid nitrogen and exposure to air, diluted with THF, and passed through a neutral, activated aluminum oxide column to remove copper catalyst. Subsequently, the final product was obtained by precipitation with cold methanol to remove impurities and dried at 40 °C under vacuum for 48 h.

Synthesis of Hydrophobic Starlike Poly(tert-butyl acrylate)-block-poly(methyl methacrylate) (Starlike PtBA-b-PMMA). Starlike P*t*BA, CuBr, PMDETA, MMA, and anisole (molar ratio = 1:1:2:1000:1000) were mixed in an ampule, degassed by three freeze−pump−thaw cycles in liquid nitrogen, and polymerized at 80 °C in an oil bath for the desired time. Afterward, the reaction was quenched by immersion in liquid nitrogen and then exposure to air. Then the reaction solution was diluted with THF, passed through a neutral, activated aluminum oxide column to remove the copper catalyst, precipitated with cold methanol to remove impurities, and finally dried at 40 °C in vacuum for 48 h.

Synthesis of Azide-Terminated Starlike Poly(tert-butyl acrylate) (Starlike PtBA-N_3). Starlike P*t*BA was dissolved in anhydrous DMF (10 mL) together with sodium azide (molar ratio of Br in starlike PtBA to sodium azide = 1:50). After the reaction solution was stirred for 24 h at room temperature, it was diluted with dichloromethane, washed with water five times to remove excess sodium azide, and dried with $MgSO_4$. The final product was obtained by rotary evaporation and was dried at room temperature under vacuum.

Synthesis of Alkyne-Terminated Poly(ethylene oxide) (Alkyne-Terminated PEO). Freshly cleaned potassium (120 mmol) was added to 200 mL of THF and naphthalene (120 mmol) under argon protection and stirred for 4 h, followed by the addition of 132 mmol of diphenylmethane. Afterward, the reaction temperature was slowly increased to the reflux temperature and kept there for 36 h. After the completion of the reaction, the solution was titrated with 0.1 M HCl and achieved a final concentration of diphenylmethylpottassium (DPMK) solution of 0.5 M. Subsequently, 2 mmol of poly(ethylene glycol) methyl ether (Mn ∼ 5000 g/mol) was added to 60 mL of THF, followed by the addition of DPMK solution at 0 °C under argon protection. After the solution was stirred for 1 h, 10 mmol of propargyl bromide was added using a syringe pump for 2 h. Subsequently, the reaction solution was stirred at room temperature for 24 h to complete the reaction. Finally, the pure product was obtained by evaporating all the remaining solvents via rotary evaporation and washing with diethyl ether twice, yielding a white powderlike sample.

Synthesis of Amphiphilic Starlike Poly(tert-butyl acrylate)-block-poly(ethylene oxide) (Starlike PtBA-b-PEO). One gram of starlike PtBA was dissolved in 40 mL of dichloromethane, followed by the addition of 0.5 g of alkyne-terminated PEO. After the mixture was purged with argon for 30 min, CuBr and PMDETA (molar ratio = 1:2) were added to the mixture. Afterward, the solution was stirred at room temperature for 24 h to complete the reaction. Subsequently, copper catalyst in the mixture was removed by passing the mixture through a neutral, activated aluminum oxide column. The final product was obtained by removing the solvent with rotary evaporation, washed with diethyl ether three times, and dried in vacuum for 48 h at room temperature.

Synthesis of Amphiphilic Starlike Poly(acrylic acid)-block-polystyrene (Starlike PAA-b-PS). Typically, 200 mg of starlike P*t*BA-*b*-PS block copolymers was added to 40 mL of anhydrous dichloromethane and 2 mL of TFA and stirred continuously for 24 h at room temperature to complete the hydrolysis of the P*t*BA. Afterward, a white-powder-like product was obtained by rotary evaporation to remove excess TFA, redissolved in DMF, precipitated in cold methanol, filtered, and dried at room temperature in vacuum.

Synthesis of Amphiphilic Starlike Poly(acrylic acid)-block-poly(methyl methacrylate) (Starlike PAA-b-PMMA). Starlike PAA-*b*-

https://doi.org/10.1021/acs.chemmater.1c01132
Chem. Mater. 2021, 33, 6701−6712

PMMA was synthesized in a manner similar to starlike PAA-*b*-PS via hydrolysis of P*t*BA-*b*-PMMA as described above.

Synthesis of Hydrophilic Starlike Poly(acrylic acid)-block-poly(ethylene oxide) (Starlike PAA-b-PEO). Starlike PAA-*b*-PEO was synthesized in a manner similar to starlike PAA-*b*-PS as described above.

Synthesis of Linear Poly(acrylic acid)-block-polystyrene (Linear PAA-b-PS). Linear PAA-*b*-PS was synthesized in a manner similar to starlike PAA-*b*-PS via sequential ATRP and hydrolysis of inner P*t*BA block, except for replacement of the Br-*β*-CD macroinitiator with linear initiator EBiB.

Synthesis of PbSe Nanoparticles (NPs) by Capitalizing on Starlike Block Copolymers as Nanoreactors. TOP-Se was prepared by dissolving 2 mmol of selenium powder in 10 mL of TOP at room temperature via ultrasonication. Afterward, 10 mg of starlike block copolymer nanoreactors (i.e., PAA-*b*-PS or PAA-*b*-PMMA or PAA-*b*-PEO) was dissolved in 9 mL of anhydrous DMF together with 0.2 mmol of $Pb(NO_3)_2$ and 1 mL of TOP-Se solution under stirring. For PS-ligated and PMMA-ligated PbSe NPs, 1 mL of BA was added to the mixture under argon protection. For PEO-ligated PbSe NPs, 1 mL of DPE was added to the mixture under argon protection. Subsequently, the mixture was stirred at 60 °C for 2 h to ensure selective partitioning of precursors within the regime occupied by PAA blocks, followed by heating at 160 °C for 4 h under argon protection, yielding a homogeneous brown colloidal solution. For isolation and purification of PbSe NPs, for PMMA-ligated and PS-ligated PbSe NPs, the crude reaction solution was first mixed with an equal volume of ethanol/hexane mixture solution (poor solvent) (the volume ratio of ethanol to hexane = 1:1), followed by centrifugation and redissolution in toluene (good solvent). After the NPs were washed three times, the purified PbSe NPs were redissolved in TCE rather than toluene for characterization. For PEO-ligated PbSe NPs, the ethanol/hexane mixture solution (i.e., poor solvents) was replaced with diethyl ether/hexane (the volume ratio of diethyl ether to hexane = 2:1). After centrifugation, the precipitated PEO-ligated PbSe NPs were redissolved in toluene two additional times and washed using diethyl ether/hexane as poor solvents and toluene as the good solvent. Finally, the purified PEO-ligated PbSe NPs were dissolved in TCE for characterization.

Synthesis of CdSe and PbTe NPs by Capitalization on Starlike Block Copolymer as Nanoreactors. The synthesis of CdSe NPs was similar to that of PbSe NPs using starlike PAA-*b*-PS block copolymers as nanoreactors, except for replacement of $Pb(NO_3)_2$ with $Cd(NO_3)_2$.

The synthesis of PbTe NPs was similar to that of PbSe NPs using starlike PAA-*b*-PS block copolymers as nanoreactors, except for replacement of the TOP-Se with TOP-Te that was synthesized by dissolution of tellurium powder in TOP.

Synthesis of PbSe NPs Ligated with Conventional OA on the Surface. OA-ligated PbSe NPs were synthesized by following the literature with a minor modification.[22] Typically, 1 mmol of $Pb(NO_3)_2$ was added to the mixture of 10 mL of OA and 30 mL of ODE to form a lead precursor solution, degassed at 120 °C for 2 h, and then protected by an argon atmosphere. On the other hand, 0.05 mmol of selenium powder was dissolved in 40 mL of TOP to form TOP-Se. Afterward, the TOP-Se was injected into the lead precursor solution at 180 °C. After 90 s, the reaction was quenched by immersion in an ice bath. The OA-ligated PbSe NPs were then isolated and purified by addition of a methanol/butanol mixture and then centrifugation. Finally, the purified OA-ligated PbSe NPs were redissolved in TCE to form a brown colloidal solution.

Characterization. The molecular weights and polydispersity indices of hydrophobic polymers were measured by GPC equipped with a G1362A refractive detector and a G1314A variable wavelength detector, one 5 μm LP gel column (500 Å, molecular range: 500−2 × 10^4 g/mol), and one 5 μm LP gel mixed bed column (molecular range: 200−3 × 10^6 g/mol), and THF as the mobile phase at a rate of 1.0 mL/min at 35 °C. The molecular weights and polydispersity indices of amphiphilic and hydrophilic polymers were measured by GPC equipped with an RID-10A refractive index detector, LC-10A pump, CTO-20A column oven, and DMF (stabilized with LiBr) as the mobile phase at a rate of 1.0 mL/min at 35 °C. Both GPCs were calibrated with monodisperse linear PS as the standard. ^{1}H NMR was measured using a Varian mercury 400 nuclear magnetic resonance spectroscopy with either $CDCl_3$ or DMF-d_7 as solvent. Fourier transform infrared spectra (FT-IR) were obtained by using a Nicolet 6700 FT-IR spectrometer. The hydrodynamic sizes of block copolymer micelles were characterized by using dynamic light scattering (Wyatt DynaPro) with DMF as the solvent at 25 °C. X-ray diffraction profiles were collected with a Panalytical Empyrean XRD system. The morphologies of the as-prepared NPs were investigated using an Hitachi HT7700 transmission electron microscope (TEM) operated at 120 kV. The high-resolution TEM image and energy-dispersive X-ray analysis of the samples was acquired with an Hitachi 2700 TEM. The UV−vis−NIR spectra were recorded using a Shimadzu UV-2600 and Cary 5000 UV−vis−NIR spectrometers. The NIR photoluminescence spectra were collected via a Shimadzu RF-5301PC spectrofluorophotometer with TCE as solvent. The X-ray photoelectron spectra were obtained from a Thermo K-Alpha X-ray photoelectron spectroscope.

■ ASSOCIATED CONTENT

Supporting Information

The Supporting Information is available free of charge at https://pubs.acs.org/doi/10.1021/acs.chemmater.1c01132.

Additional figures and tables: Figures S1−S23 and Tables S1−S3, including ^{1}H NMR, GPC, DLS, TEM, EDS, FT-IR, XRD, XPS, optical characterizations, and digital photographs (PDF)

■ AUTHOR INFORMATION

Corresponding Author

Zhiqun Lin − *School of Materials Science and Engineering, Georgia Institute of Technology, Atlanta, Georgia 30332, United States;* orcid.org/0000-0003-3158-9340; Email: zhiqun.lin@mse.gatech.edu

Authors

Shuang Liang − *School of Materials Science and Engineering and School of Chemical and Biomolecular Engineering, Georgia Institute of Technology, Atlanta, Georgia 30332, United States*

Mingyue Zhang − *School of Materials Science and Engineering, Georgia Institute of Technology, Atlanta, Georgia 30332, United States*

Yanjie He − *School of Materials Science and Engineering, Georgia Institute of Technology, Atlanta, Georgia 30332, United States*

Zhitao Kang − *School of Materials Science and Engineering and Georgia Tech Research Institute, Georgia Institute of Technology, Atlanta, Georgia 30332, United States;* orcid.org/0000-0001-6736-7809

Mengkun Tian − *The Institute for Electronics and Nanotechnology, Georgia Institute of Technology, Atlanta, Georgia 30332, United States;* orcid.org/0000-0003-2790-7799

Meng Zhang − *School of Materials Science and Engineering, Georgia Institute of Technology, Atlanta, Georgia 30332, United States*

Han Miao − *School of Materials Science and Engineering, Georgia Institute of Technology, Atlanta, Georgia 30332, United States*

Complete contact information is available at: https://pubs.acs.org/10.1021/acs.chemmater.1c01132

Notes

The authors declare no competing financial interest.

■ ACKNOWLEDGMENTS

This work is supported by the Air Force Office of Scientific Research (FA9550-19-1-0317) and the National Science Foundation (CBET 1803495 and CMMI 1914713).

■ REFERENCES

(1) Kershaw, S. V.; Susha, A. S.; Rogach, A. L. Narrow bandgap colloidal metal chalcogenide quantum dots: synthetic methods, heterostructures, assemblies, electronic and infrared optical properties. *Chem. Soc. Rev.* **2013**, *42* (7), 3033−3087.

(2) Talapin, D. V.; Murray, C. B. PbSe nanocrystal solids for n-and p-channel thin film field-effect transistors. *Science* **2005**, *310* (5745), 86−89.

(3) Moreels, I.; Lambert, K.; Smeets, D.; De Muynck, D.; Nollet, T.; Martins, J. C.; Vanhaecke, F.; Vantomme, A.; Delerue, C.; Allan, G.; Hens, Z. Size-dependent optical properties of colloidal PbS quantum dots. *ACS Nano* **2009**, *3* (10), 3023−3030.

(4) Redl, F. X.; Cho, K.-S.; Murray, C. B.; O'Brien, S. Three-dimensional binary superlattices of magnetic nanocrystals and semiconductor quantum dots. *Nature* **2003**, *423* (6943), 968−971.

(5) Yoon, Y. J.; Chang, Y.; Zhang, S.; Zhang, M.; Pan, S.; He, Y.; Lin, C. H.; Yu, S.; Chen, Y.; Wang, Z.; Ding, Y.; Jung, J.; Thadhani, N.; Tsukruk, V. V.; Kang, Z.; Lin, Z. Enabling Tailorable Optical Properties and Markedly Enhanced Stability of Perovskite Quantum Dots by Permanently Ligating with Polymer Hairs. *Adv. Mater.* **2019**, *31* (32), 1901602.

(6) He, M.; Li, B.; Cui, X.; Jiang, B.; He, Y.; Chen, Y.; O'Neil, D.; Szymanski, P.; Ei-Sayed, M. A.; Huang, J.; Lin, Z. Meniscus-assisted solution printing of large-grained perovskite films for high-efficiency solar cells. *Nat. Commun.* **2017**, *8* (1), 16045.

(7) Semonin, O. E.; Luther, J. M.; Choi, S.; Chen, H.-Y.; Gao, J.; Nozik, A. J.; Beard, M. C. Peak external photocurrent quantum efficiency exceeding 100% via MEG in a quantum dot solar cell. *Science* **2011**, *334* (6062), 1530−1533.

(8) Koh, Y. K.; Vineis, C.; Calawa, S.; Walsh, M.; Cahill, D. G. Lattice thermal conductivity of nanostructured thermoelectric materials based on PbTe. *Appl. Phys. Lett.* **2009**, *94* (15), 153101.

(9) Wang, R. Y.; Feser, J. P.; Lee, J.-S.; Talapin, D. V.; Segalman, R.; Majumdar, A. Enhanced thermopower in PbSe nanocrystal quantum dot superlattices. *Nano Lett.* **2008**, *8* (8), 2283−2288.

(10) Sukhovatkin, V.; Hinds, S.; Brzozowski, L.; Sargent, E. H. Colloidal quantum-dot photodetectors exploiting multiexciton generation. *Science* **2009**, *324* (5934), 1542−1544.

(11) Wise, F. W. Lead salt quantum dots: the limit of strong quantum confinement. *Acc. Chem. Res.* **2000**, *33* (11), 773−780.

(12) Ellingson, R. J.; Beard, M. C.; Johnson, J. C.; Yu, P.; Micic, O. I.; Nozik, A. J.; Shabaev, A.; Efros, A. L. Highly efficient multiple exciton generation in colloidal PbSe and PbS quantum dots. *Nano Lett.* **2005**, *5* (5), 865−871.

(13) Evers, W. H.; Schins, J. M.; Aerts, M.; Kulkarni, A.; Capiod, P.; Berthe, M.; Grandidier, B.; Delerue, C.; Van Der Zant, H. S. J.; Van Overbeek, C.; Peters, J. L.; Vanmaekelbergh, D.; Siebbeles, L. D. A. High charge mobility in two-dimensional percolative networks of PbSe quantum dots connected by atomic bonds. *Nat. Commun.* **2015**, *6*, 8195.

(14) Lian, L.; Xia, Y.; Zhang, C.; Xu, B.; Yang, L.; Liu, H.; Zhang, D.; Wang, K.; Gao, J.; Zhang, J. In situ tuning the reactivity of selenium precursor to synthesize wide range size, ultralarge-scale, and ultrastable PbSe quantum dots. *Chem. Mater.* **2018**, *30* (3), 982−989.

(15) Du, H.; Chen, C.; Krishnan, R.; Krauss, T. D.; Harbold, J. M.; Wise, F. W.; Thomas, M. G.; Silcox, J. Optical properties of colloidal PbSe nanocrystals. *Nano Lett.* **2002**, *2* (11), 1321−1324.

(16) Grimaldi, G.; Crisp, R. W.; Ten Brinck, S.; Zapata, F.; Van Ouwendorp, M.; Renaud, N.; Kirkwood, N.; Evers, W. H.; Kinge, S.; Infante, I.; Siebbeles, L. D. A.; Houtepen, A. J. Hot-electron transfer in quantum-dot heterojunction films. *Nat. Commun.* **2018**, *9*, 2310.

(17) Liu, Y.; Li, F.; Shi, G.; Liu, Z.; Lin, X.; Shi, Y.; Chen, Y.; Meng, X.; Lv, Y.; Deng, W.; Pan, X.; Ma, W. PbSe quantum dot solar cells based on directly synthesized semiconductive Inks. *ACS Energy Lett.* **2020**, *5*, 3797−3803.

(18) Sykora, M.; Koposov, A. Y.; McGuire, J. A.; Schulze, R. K.; Tretiak, O.; Pietryga, J. M.; Klimov, V. I. Effect of air exposure on surface properties, electronic structure, and carrier relaxation in PbSe nanocrystals. *ACS Nano* **2010**, *4* (4), 2021−2034.

(19) Pietryga, J. M.; Werder, D. J.; Williams, D. J.; Casson, J. L.; Schaller, R. D.; Klimov, V. I.; Hollingsworth, J. A. Utilizing the lability of lead selenide to produce heterostructured nanocrystals with bright, stable infrared emission. *J. Am. Chem. Soc.* **2008**, *130* (14), 4879−4885.

(20) Bae, W. K.; Joo, J.; Padilha, L. A.; Won, J.; Lee, D. C.; Lin, Q.; Koh, W.-k.; Luo, H.; Klimov, V. I.; Pietryga, J. M. Highly effective surface passivation of PbSe quantum dots through reaction with molecular chlorine. *J. Am. Chem. Soc.* **2012**, *134* (49), 20160−20168.

(21) Zhang, J.; Gao, J.; Miller, E. M.; Luther, J. M.; Beard, M. C. Diffusion-controlled synthesis of PbS and PbSe quantum dots with in situ halide passivation for quantum dot solar cells. *ACS Nano* **2014**, *8* (1), 614−622.

(22) Peters, J. L.; Van Der Bok, J.; Hofmann, J. P.; Vanmaekelbergh, D. Hybrid oleate−Iodide ligand shell for air-stable PbSe nanocrystals and superstructures. *Chem. Mater.* **2019**, *31* (15), 5808−5815.

(23) Woo, J. Y.; Lee, S.; Lee, S.; Kim, W. D.; Lee, K.; Kim, K.; An, H. J.; Lee, D. C.; Jeong, S. Air-stable PbSe nanocrystals passivated by phosphonic acids. *J. Am. Chem. Soc.* **2016**, *138* (3), 876−883.

(24) Antanovich, A.; Achtstein, A.; Matsukovich, A.; Prudnikau, A.; Bhaskar, P.; Gurin, V.; Molinari, M.; Artemyev, M. A strain-induced exciton transition energy shift in CdSe nanoplatelets: the impact of an organic ligand shell. *Nanoscale* **2017**, *9* (45), 18042−18053.

(25) Pang, X.; He, Y.; Jung, J.; Lin, Z. 1D nanocrystals with precisely controlled dimensions, compositions, and architectures. *Science* **2016**, *353* (6305), 1268−1272.

(26) Xu, H.; Xu, Y.; Pang, X.; He, Y.; Jung, J.; Xia, H.; Lin, Z. A general route to nanocrystal kebabs periodically assembled on stretched flexible polymer shish. *Sci. Adv.* **2015**, *1* (2), No. e1500025.

(27) He, Y.; Yoon, Y. J.; Harn, Y. W.; Biesold-McGee, G. V.; Liang, S.; Lin, C. H.; Tsukruk, V. V.; Thadhani, N.; Kang, Z.; Lin, Z. Unconventional route to dual-shelled organolead halide perovskite nanocrystals with controlled dimensions, surface chemistry, and stabilities. *Sci. Adv.* **2019**, *5* (11), No. eaax4424.

(28) Pang, X.; Zhao, L.; Han, W.; Xin, X.; Lin, Z. A general and robust strategy for the synthesis of nearly monodisperse colloidal nanocrystals. *Nat. Nanotechnol.* **2013**, *8* (6), 426−431.

(29) Dai, Q.; Wang, Y.; Li, X.; Zhang, Y.; Pellegrino, D. J.; Zhao, M.; Zou, B.; Seo, J. T.; Wang, Y.; Yu, W. W. Size-Dependent Composition and Molar Extinction Coefficient of PbSe Semiconductor Nanocrystals. *ACS Nano* **2009**, *3* (6), 1518−1524.

(30) Allan, G.; Delerue, C. Confinement effects in PbSe quantum wells and nanocrystals. *Phys. Rev. B: Condens. Matter Mater. Phys.* **2004**, *70*, 245321.

(31) Moreels, I.; Lambert, K.; De Muynck, D.; Vanhaecke, F.; Poelman, D.; Martins, J. C.; Allan, G.; Hens, Z. Composition and Size-Dependent Extinction Coefficient of Colloidal PbSe Quantum Dots. *Chem. Mater.* **2007**, *19* (25), 6101−6106.

(32) Koole, R.; Allan, G.; Delerue, C.; Meijerink, A.; Vanmaekelbergh, G.; Houtepen, A. J. Optical Investigation of Quantum Confinement in PbSe Nanocrystals at Different Points in the Brillouin Zone. *Small* **2008**, *4* (1), 127−133.

(33) Moreels, I.; Fritzinger, B.; Martins, J. C.; Hens, Z. Surface chemistry of colloidal PbSe nanocrystals. *J. Am. Chem. Soc.* **2008**, *130* (45), 15081−15086.

(34) Peng, X.; Abelson, A.; Wang, Y.; Qian, C.; Shangguan, J.; Zhang, Q.; Yu, L.; Yin, Z.-W.; Zheng, W.; Bustillo, K. C.; Guo, X.; Liao, H.-G.; Sun, S.-G.; Law, M.; Zheng, H. In situ TEM study of the

https://doi.org/10.1021/acs.chemmater.1c01132
Chem. Mater. 2021, 33, 6701−6712

degradation of PbSe nanocrystals in Air. *Chem. Mater.* **2019**, *31* (1), 190−199.
(35) Peters, J. L.; Van den Bos, K. H. W.; Van Aert, S.; Goris, B.; Bals, S.; Vanmaekelbergh, D. Ligand-induced shape transformation of PbSe nanocrystals. *Chem. Mater.* **2017**, *29* (9), 4122−4128.
(36) Liu, H.; Guyot-Sionnest, P. Photoluminescence lifetime of lead selenide colloidal quantum dots. *J. Phys. Chem. C* **2010**, *114* (35), 14860−14863.
(37) Zherebetskyy, D.; Scheele, M.; Zhang, Y.; Bronstein, N.; Thompson, C.; Britt, D.; Salmeron, M.; Alivisatos, P.; Wang, L.-W. Hydroxylation of the surface of PbS nanocrystals passivated with oleic acid. *Science* **2014**, *344* (6190), 1380−1384.
(38) Hansen, C. M. *Hansen solubility parameters: a user's handbook*, 2nd ed.; CRC Press: New York, 2007.
(39) He, Y.; Pang, X.; Jiang, B.; Feng, C.; Harn, Y.-W.; Chen, Y.; Yoon, Y. J.; Pan, S.; Lu, C.-H.; Chang, Y.; Zebarjadi, M.; Kang, Z.; Thadhani, N.; Peng, J.; Lin, Z. Unconventional Route to Uniform Hollow Semiconducting Nanoparticles with Tailorable Dimensions, Compositions, Surface Chemistry, and Near-Infrared Absorption. *Angew. Chem., Int. Ed.* **2017**, *56* (42), 12946−12951.
(40) Xu, H.; Pang, X.; He, Y.; He, M.; Jung, J.; Xia, H.; Lin, Z. An Unconventional Route to Monodisperse and Intimately Contacted Semiconducting Organic−Inorganic Nanocomposites. *Angew. Chem., Int. Ed.* **2015**, *54* (15), 4636−4640.
(41) Li, X.; Iocozzia, J.; Chen, Y.; Zhao, S.; Cui, X.; Wang, W.; Yu, H.; Lin, S.; Lin, Z. From Precision Synthesis of Block Copolymers to Properties and Applications of Nanoparticles. *Angew. Chem., Int. Ed.* **2018**, *57* (8), 2046−2070.
(42) Liu, Y.; Wang, J.; Zhang, M.; Li, H.; Lin, Z. Polymer-Ligated Nanocrystals Enabled by Nonlinear Block Copolymer Nanoreactors: Synthesis, Properties, and Applications. *ACS Nano* **2020**, *14* (10), 12491−12521.

https://doi.org/10.1021/acs.chemmater.1c01132
Chem. Mater. 2021, 33, 6701−6712